

1
2
3
4
5
6
7
8
9
10
11
12
13
14
15
16
17
18
19
20
21
22
23
24
25
26

Age-dependent changes in electrophysiology and calcium handling – implications for pediatric cardiac research

Luther M. Swift^{1,2}, Morgan Burke^{1,2}, Devon Guerrelli^{1,2}, Manelle Ramadan^{1,2}, Marissa Reilly¹, Damon McCullough^{1,2}, Ashika Chaluvadi¹, Colm Mulvany¹, Rafael Jaimes^{1,2}, Nikki Gillum Posnack^{1,2,3}

¹ Sheikh Zayed Institute for Pediatric Surgical Innovation, Children’s National Health System, Washington DC USA 20010

² Children’s National Heart Institute, Children’s National Health System, Washington DC USA 20010

³ Department of Pediatrics, Department of Pharmacology & Physiology, School of Medicine and Health Sciences: George Washington University, Washington DC USA 20037

Short Title: Cardiac development

Corresponding author:

Nikki Gillum Posnack, Ph.D.
Sheikh Zayed Institute, 6th floor, M7707
111 Michigan Avenue, NW
Washington, DC, USA 20010
Tel: (202) 476-2475
Email: nposnack@childrensnational.org

27 **ABSTRACT**

28
29

30 **Rationale:** The heart continues to develop and mature after birth and into adolescence. Accordingly,
31 cardiac maturation is likely to include a progressive refinement in both organ morphology and function
32 during the postnatal period. Yet, age-dependent changes in cardiac electrophysiology and calcium
33 handling have not yet been fully characterized.

34 **Objective:** The objective of this study, was to examine the relationship between cardiac maturation,
35 electrophysiology, and calcium handling throughout postnatal development in a rat model.

36 **Methods:** Postnatal rat cardiac maturation was determined by measuring the expression of genes
37 involved in cell-cell coupling, electrophysiology, and calcium handling. In vivo electrocardiograms were
38 recorded from neonatal, juvenile, and adult animals. Simultaneous dual optical mapping of
39 transmembrane voltage and calcium transients was performed on isolated, Langendorff-perfused rat
40 hearts (postnatal day 0–3, 4-7, 8-14, adult).

41 **Results:** Younger, immature hearts displayed slowed electrical conduction, prolonged action potential
42 duration and increased ventricular refractoriness. Slowed calcium handling in the immature heart
43 increased the propensity for calcium transient alternans which corresponded to alterations in the
44 expression of genes encoding calcium handling proteins. Developmental changes in cardiac
45 electrophysiology were associated with the altered expression of genes encoding potassium channels
46 and intercalated disc proteins.

47 **Conclusion:** Using an intact whole heart model, this study highlights chronological changes in cardiac
48 electrophysiology and calcium handling throughout postnatal development. Results of this study can
49 serve as a comprehensive baseline for future studies focused on pediatric cardiac research, safety
50 assessment and/or preclinical testing using rodent models.

51

52 **Keywords:**

53 Cardiac maturation, optical mapping, electrophysiology, calcium handling, excitation-contraction
54 coupling

55

56 INTRODUCTION

57 The mammalian heart begins as a mesoderm derived tube with slow electrical conduction, an
58 underdeveloped sarcoplasmic reticulum and limited contractile force (van Weerd & Christoffels, 2016;
59 Günthel *et al.*, 2018). The mammalian heart continues to develop postnatally, not reaching maturity in
60 small rodents until weeks after birth (Vreeker *et al.*, 2014). Because of this extended period of
61 maturation, the juvenile heart is uniquely dynamic and often considered a ‘moving target’ (Pesco-
62 Koplowitz *et al.*, 2018). As such, there are considerable gaps in our understanding of normal cardiac
63 physiology throughout the postnatal period. These gaps in knowledge can have unintended
64 consequences, particularly when pharmacological therapies or toxicological studies are designed and
65 tested using adult cardiac models – targeting ion channels and/or signaling pathways that may be
66 underdeveloped in the immature myocardium. Indeed, a number of age-dependent cardiac responses
67 to antiarrhythmics have been reported (e.g., dofetilide (Obreztkikova *et al.*, 2003), sotalol (Saul *et al.*,
68 2001)) and inotropes (e.g., dobutamine, isoproterenol (Driscoll *et al.*, 1980)). Likewise, the Cardiac
69 Safety Research Consortium recently highlighted the need for research studies focused on
70 developmental cardiac physiology, with the goal of improving cardiac safety testing. Specifically, the
71 consortium emphasized a need for “functional, systematic and comprehensive studies of cardiac
72 development” to bolster pediatric cardiac research (Bates *et al.*, 2012).

73
74 Small rodent animal models are frequently employed in cardiovascular research, as the rodent and
75 human heart follow a similar sequence of structural cardiac development and electrophysiological
76 patterning (Marcela *et al.*, 2012; Krishnan *et al.*, 2014; van Weerd & Christoffels, 2016). As with
77 humans, the rodent heart exhibits electrical restitution properties and an action potential that is rate-
78 dependent (Knollmann *et al.*, 2007). Immature cardiac myocytes from both humans and rodents lack
79 fully developed transverse tubules and sarcoplasmic reticulum (Ziman *et al.*, 2010), which influences
80 calcium cycling (Escobar *et al.*, 2004; Wagner *et al.*, 2005) and contractile function (Louch *et al.*, 2015;
81 Racca *et al.*, 2016). Additionally, immature rodent and human cardiomyocytes have underdeveloped
82 intercalated discs, which impacts cell-cell coupling and electrical conduction (Vreeker *et al.*, 2014).
83 Moreover, age-dependent changes in voltage-gated potassium (Wahler *et al.*, 1994; Wang & Duff,
84 1997; Grandy *et al.*, 2007), calcium (Wang *et al.*, 2003; Wagner *et al.*, 2005) and sodium channel (Cai
85 *et al.*, 2011) current have been described. Although species-specific characteristics do exist; for
86 instance an age-dependent increase in the heart rate of small rodents (Heier *et al.*, 2010) is coupled to
87 changes in excitation-contraction coupling that allow the rodent heart to adapt to faster beating rates.
88 Accordingly, the rodent action potential (measured via intracellular microelectrode) becomes
89 progressively shorter as cardiomyocytes mature (Escande *et al.*, 1985; Wahler *et al.*, 1994; Wang *et al.*,
90 2003). Nevertheless, small rodents remain a vital tool to investigate cardiac maturation,
91 electrophysiology and excitation-contraction coupling (Krishnan *et al.*, 2014; Günthel *et al.*, 2018).

92

93 The objective of this study was to evaluate the relationship between cardiac maturation,
94 electrophysiology and calcium handling throughout postnatal rat development. To date, developmental
95 changes in rodent cardiac electrophysiology and calcium handling have largely been limited to cell
96 models (Artman *et al.*, 2000). However, the results gleaned from these models may not translate to a
97 whole heart with specialized anatomy, cell populations (atrial, nodal, ventricular), spatial tissue
98 heterogeneity, and a coordinated conduction system. Therefore, we utilized a three-dimensional whole
99 heart model to describe temporal changes in rat cardiac electrophysiology and calcium handling during
100 postnatal development. Simultaneous, dual-optical mapping of transmembrane voltage (V_m) and
101 calcium transients (Ca^{2+}) was performed on isolated Langendorff-perfused hearts. The results of this
102 study can serve as a baseline for future pediatric cardiac research studies, focused on environmental,
103 pharmacological or toxicological perturbations.

104

105

METHODS

106 Animal protocols were approved by the Institutional Animal Care and Use Committee at Children's
107 Research Institute and followed the National Institutes of Health's *Guide for the Care and Use of*
108 *Laboratory Animals*. Experiments were performed using Sprague-Dawley rats from postnatal day
109 (PND) 0 to adulthood (2-3 months), Taconic Biosciences (n = 126). Animals were housed in
110 conventional acrylic rat cages in the Research Animal Facility, under standard environmental conditions
111 (12:12 hour light:dark cycle, 64 – 78°C, 30-70% humidity, free access to reverse osmosis water, corn
112 cob bedding and #2918 rodent chow, Envigo).

113

In vivo surface electrocardiogram recordings

115 Electrocardiograms (ECG) were collected from conscious animals using an ecgTUNNEL system (emka
116 Technologies). The platform electrodes were coated with ultrasound gel prior to placing the animal in
117 the system. A clear half-tunnel was carefully positioned over the top of older animals (>pnd 6), to limit
118 movement which can introduce noise in the signal. The animals were acclimated to the platform for 5
119 min, biosignals were continuously acquired for 2 min using iox2 (emka Technologies), and ECG
120 segments were computed in ecgAUTO (emka Technologies).

121

Isolated heart preparation and electrophysiology measurements

123 Animals were anesthetized with 2% isoflurane; the heart was rapidly excised, and the aorta cannulated.
124 The heart was then transferred to a temperature-controlled (37°C) constant-pressure (70 mmHg)
125 Langendorff perfusion system. Excised hearts were perfused with Krebs-Henseleit buffer bubbled with
126 5% CO² and 95% oxygen throughout the duration of the experiment, as previously described (~1 hour)
127 (Jaimes III *et al.*, 2014). Electrocardiograms were recorded throughout the duration of the experiment in

128 a lead II configuration. During sinus rhythm, ECG signals were collected to analyze heart rate, atrial
129 depolarization, atrioventricular conduction (PR interval), ventricular depolarization time (QRS width),
130 and heart rate variability, including root means successive square difference (rMSSD) and standard
131 deviation of the normal RR intervals (SDNN). Signals were acquired in iox2 and ECG parameters were
132 quantified in ecgAUTO.

133

134 **Optical mapping**

135 To reduce motion artifact during imaging experiments, the heart was perfused with Krebs-Henseleit
136 buffer supplemented with 10 μ M (-/-) blebbistatin (Sigma-Aldrich) (Fedorov *et al.*, 2007; Swift *et al.*,
137 2012). Epicardial imaging was performed by sequentially loading the heart with fluorescent dyes
138 through a bubble trap located proximal to the aortic cannula (Kay *et al.*, 2008; Posnack *et al.*, 2014a). A
139 calcium indicator dye (50 μ g Rhod2-AM) (Lang *et al.*, 2011; Jaimes *et al.*, 2016a) was added and
140 allowed to stabilize for 10 min, followed by a potentiometric dye (62.1 μ g RH237) (Swift *et al.*, 2008).
141 The epicardium was illuminated with an LED spotlight (530 nm, 200 mW; Mightex), fitted with an optical
142 filter (ET530/40x nm, Chroma Technologies). Fluorescence signals were acquired using an image
143 splitting device (Optosplit II, Cairn Research Ltd) positioned in front of a sCMOS camera (Zyla 4.2Plus,
144 Andor Technologies). The path splitter was configured with a dichroic mirror (660+nm, Chroma
145 Technologies) that passed RH237 emission and reflected Rhod-2AM fluorescence. RH237
146 fluorescence was longpass filtered (ET710, Chroma Technologies) and Rhod-2AM was bandpass
147 filtered (ET585/40m, Chroma Technologies). A fixed focal length 17mm/F0.95 lens was attached to the
148 image splitting device (Schneider, #21-010456). *MetaMorph* (Molecular Devices LLC) was used for
149 optosplit image alignment and LED on/off triggering. Transmembrane voltage and calcium signals were
150 acquired simultaneously at 800 frames per second.

151

152 For ventricular pacing, a 0.25 mm diameter tungsten, unipolar, cathodal electrode was placed on the
153 left ventricle's epicardium, and a stainless-steel indifferent electrode was placed under the heart. To
154 determine the ventricular effective refractory period (VERP), dynamic pacing (S1-S1) was performed
155 during optical mapping. A Bloom Classic electrophysiology stimulator (Fisher Medical) was set at a
156 pacing current 1.5x the minimum pacing threshold (~1.8 mA) with 1 msec monophasic pulses; pacing
157 cycle length (PCL) was decremented stepwise (250 – 50 msec) until a loss of capture was observed, in
158 order to identify VERP.

159

160 **Signal Processing**

161 Following image acquisition, signal processing and data analysis were performed using a custom
162 MATLAB script, as previously described (Posnack *et al.*, 2014b; Jaimes *et al.*, 2016b). A region of
163 interest (appx 0.75 mm) was selected in identical locations on the split image of the heart for each raw

164 image. The signals from each ROI corresponding to transmembrane voltage and calcium transients,
165 were independently averaged and plotted against time. A peak detector algorithm was applied, and
166 characteristics of each waveform were measured and averaged, including: action potential duration at
167 30% (APD30) and 80% (APD80) repolarization, APD triangulation (APD80-APD30) (Hondeghe *et al.*,
168 2001), and calcium transient duration at 30% (CaD30) and 80% (CaD80) reuptake. Optical signals
169 were acquired during each pacing cycle length (PCL). Calcium transient alternans were defined as
170 sequential calcium transient measurements that differed by >5%.

171

172 **Gene Expression Analysis**

173 Total RNA was isolated from heart tissue using a RNeasy fibrous tissue kit (Qiagen). RNA was reverse
174 transcribed using a SuperScript VILO cDNA kit (Thermo Scientific), and Taqman gene expression
175 assays (Thermo Scientific) were used for quantitative real-time PCR (qPCR) analysis via a Quantstudio
176 7 platform (Applied Biosystems). Relative gene expression was assessed by normalizing CT values
177 (dCT) to the housekeeping gene glyceraldehyde-3-phosphate dehydrogenase (*GAPDH*), wherein a
178 dCT >0 indicates reduced expression relative to the housekeeping gene and dCT <0 indicates
179 increased expression relative to the housekeeping gene. dCT values allow for comparison between
180 genes of interest, as compared to fold-change measurements. dCT values are reported as an average
181 of technical replicates, with each assay including a minimum of 3 individual biological replicates.

182

183 Genes of interest include: myosin heavy chain 7 (*MYH7*), myosin heavy chain 6 (*MYH6*), gap junction
184 protein α 1 (*GJA1*), desmoplakin (*DSP*), junctophilin 2 (*JPH2*), junction plakoglobin (*JUP*), n-cadherin
185 (*CDH2*), caveolin-3 (*CAV3*), tight junction protein 1 (*TJP1*), SERCA Ca²⁺-ATPase (*SERCA2*),
186 calsequestrin 2 (*CASQ2*), ryanodine receptor 2 (*RYR2*), sodium-calcium exchanger 1 (*SLC8A1*),
187 voltage-dependent T-type calcium channel α -1G (*CACNA1G*), voltage-gated potassium channel
188 subunit Kv4.2 (*KCND2*), voltage-gated potassium channel subunit Kv1.5 (*KCNA5*), voltage-gated
189 potassium channel subunit Kv4.3 (*KCND3*), and cardiac inward rectifier potassium channel (*KCNJ2*).

190

191 **Statistical Analysis**

192 Data are presented as mean \pm standard deviation. Statistical analysis was performed using one or two-
193 way analysis of variance and false discovery rate (0.1) to correct for multiple comparisons testing using
194 GraphPad Prism. Significance was defined as (* $p \leq 0.05$). Optical signals were analyzed using custom
195 algorithms (MATLAB). Optical signals were collected for 2 seconds per pacing frequency, resulting in 8
196 – 25 signals per group.

197

198 **RESULTS**

199 *Postnatal heart development and in vivo electrophysiology*

200 The postnatal heart maintains limited proliferative potential, progressing from hyperplasia to
201 hypertrophic growth shortly after birth (**Figure 1A-D**) (Li *et al.*, 1996). In rodents, this time course is
202 associated with a shift in myosin heavy chain expression (*MYH7* to *MYH6*) and an age-dependent
203 increase in the spontaneous beating rate (Mahdavi *et al.*, 1984). We observed a similar shift in
204 expression, compared to immature hearts collected on postnatal day 0-3 (PND 0-3), *MYH7* expression
205 decreased by 96% and 155% in older hearts (PND 4-10, PND >10, respectively). Whereas *MYH6*
206 expression increased by 56% and 222% in older hearts (PND 4-10, PND >10, respectively) compared
207 with PND 0-3, **Figure 1D**. Myosin heavy chain isoform expression complements changes in heart rate,
208 as *MYH6* kinetics are three times faster than *MYH7* (Galler *et al.*, 2002). As cardiac development
209 progressed, the temporal change in *MYH* expression corresponded with a linear increase in the *in vivo*
210 resting heart rate from 181 BPM (PND 0) to 429 BPM (PND 10), **Figure 2B**. No significant difference in
211 resting heart rate was observed in animals older than PND 10. Continued development of autonomic
212 influences (Robinson, 1996) on the heart were measured via time-domain indices of heart rate
213 variability. Compared to the earliest time point (PND 0), standard deviation of heart rate (SDNN)
214 increased by 347% and 849% in older animals (PND 10 and adult, respectively), **Figure 2C**. Similarly,
215 the root means successive square difference (rMSSD) increased by 145% and 689% in older animals
216 (PND 10 and adult, respectively) compared with the earliest time point measured (PND 0), **Figure 2D**.

217
218 Along with an age-dependent increase in heart rate, we observed a progressive shortening of *in vivo*
219 electrocardiogram parameters during sinus rhythm. Atrial conduction (P-wave duration) decreased from
220 22.1 msec (PND 0) to 16.6 msec (PND 10), and atrioventricular conduction time (PR interval)
221 shortened from 93.8 msec (PND 0) to 48.1 msec (PND 10), **Figure 2A,E,F**. An age-dependent trend in
222 ventricular depolarization time (QRS interval) using non-invasive electrocardiogram monitoring was not
223 observed (**Figure 2G**). Age-dependent shortening of atrial and atrioventricular conduction can be partly
224 attributed to remodeling of cardiomyocyte size (Spach *et al.*, 2000) and more defined intercellular
225 connections (Vreeker *et al.*, 2014), which have both been shown to enhance electrical propagation.
226 Compared with immature hearts (PND 0-3), older hearts (PND >10) had an increased expression of
227 cell coupling genes encoding gap junction (39% *GJA1*) and desmosomal proteins (99% *DSP*, 24%
228 *JPH2*, 14% *JUP*), **Figure 1D**.

229 Age-dependent shortening of action potential duration and refractory period

230 Compared with neonatal cardiomyocytes, adult cells have increased potassium channel expression that
231 can expedite repolarization and shorten action potential duration (APD) time (Escande *et al.*, 1985;
232 Wahler *et al.*, 1994; Wang *et al.*, 2003). To evaluate action potential shape and duration in the whole
233 heart, transmembrane voltage signals were recorded from the epicardial surface of isolated,
234 Langendorff-perfused hearts. Optical signals acquired from juvenile hearts were binned into three age

235 groups (PND 0-3, PND 4-7, and PND 8-14) and compared with adults. Prolonged APDs were
236 consistently observed in younger hearts at multiple pacing frequencies. At 250 msec PCL, APD30
237 shortened from 54.4 msec to 20 msec and APD80 shortened from 113.2 msec to 60.5 msec (PND 0-3
238 vs adult, respectively), **Figure 3A-C**. At faster pacing rates (150msec PCL), APD30 and APD80
239 prolongation was observed in younger hearts, albeit the difference between intermediate age groups
240 was modest. Additionally, triangulation of action potential shape was more pronounced in younger
241 hearts (58.4 msec, PND 0-3) compared to older hearts (30.4 msec, adult), **Figure 3D**.

242
243 Increased potassium channel current can be mechanistically linked to shorter, less triangulated action
244 potentials (Grandy *et al.*, 2007). We observed an age-dependent increase in potassium channel gene
245 expression during postnatal cardiac maturation. This included a 17% increase in KCND2 and 18%
246 increase in KCND3 gene expression (PND 0-3 vs adult hearts), which corresponds to the fast transient
247 outward I_{t_0} current (**Figure 3F**). Importantly, I_{t_0} is responsible for the rapid repolarization and lack of a
248 plateau phase in the adult rodent action potential (Wang & Duff, 1997; Knollmann *et al.*, 2007). To
249 further investigate the relationship between potassium channel expression and action potential duration
250 time in the immature heart, an epicardial pacing protocol was implemented to pinpoint the ventricular
251 effective refractory period (VERP). The VERP shortened with increasing age, from 183 msec in
252 younger hearts (PND 0-3) to 115 msec in adult hearts (**Figure 4A-C**). With increased ventricular
253 refractoriness in younger hearts, loss of capture at PCLs <150 msec prevented APD measurements at
254 faster pacing frequencies.

255 256 Age-dependent alterations in calcium handling and incidence of alternans

257 Cardiomyocyte maturation includes the invagination of transverse tubules, formation of couplons and
258 synchronized calcium-induced calcium release (Ziman *et al.*, 2010). To evaluate calcium handling in the
259 whole heart, calcium transients were recorded from the epicardial surface of isolated Langendorff-
260 perfused hearts. Rate adaptation of the calcium transient duration time was observed in all age groups.
261 For example, in the PND0-3 age group CaD80 decreased from 168 to 151 to 133 msec (PCLs = 250,
262 200, 150msec). But, immature hearts had consistently slower calcium handling at each pacing cycle. At
263 slower pacing frequencies (250 msec PCL), CaD30 shortened from 95 msec to 57 msec and CaD80
264 shortened from 168 msec to 115 msec (PND 0-3 vs adult), **Figure 5A-C**. At faster pacing cycles (150
265 msec), CaD30 and CaD80 were longer in younger hearts, but differences between age groups were
266 modest.

267
268 Faster calcium handling in adult hearts was linked to an age-dependent increase in genes associated
269 with calcium binding within the sarcoplasmic reticulum (55% increase CASQ2 vs PND 0-3), calcium
270 release (49% increase RYR2 vs PND 0-3), and calcium-reuptake into the sarcoplasmic reticulum

271 (SERCA2), **Figure 5D**. Whereas immature cardiomyocytes rely less on calcium-induced calcium
272 release, and more on sarcolemma calcium influx via the sodium-calcium exchanger (NCX) and T-type
273 calcium channels (CACNA1G) (Louch *et al.*, 2015). In older hearts, we observed a 36% decrease in
274 NCX expression and 43% decrease in CACNA1G compared with hearts aged PND 0-3, **Figure 5D**.
275 Disturbances in calcium handling have also been associated with an increased incidence of alternans,
276 or beat-to-beat alterations in calcium transient amplitude and kinetics (Edwards & Blatter, 2014;
277 Ramadan *et al.*, 2018). A dynamic pacing protocol was implemented to pinpoint the alternans
278 threshold, or, the longest pacing cycle length required to elicit calcium transient alternans. Immature
279 hearts displayed an increased propensity for calcium transient alternans at slower pacing frequencies
280 (160 msec, PND 0-3) compared with adult hearts (99 msec), **Figure 6A, B**.

281 **DISCUSSION**

282 Cardiac excitation-contraction coupling is the process by which an action potential evokes an increase
283 in intracellular calcium, which subsequently triggers contraction (for review(Bers, 2001)). As the heart
284 continues to develop postpartum, cardiac electrophysiology and excitation-contraction coupling
285 dynamics mature with age. This occurs around 21 days postnatal in rats (van Weerd & Christoffels,
286 2016) and 20 years postnatal in humans (Mollova *et al.*, 2013) . In this study, we examined the
287 relationship between postnatal age, cardiac electrophysiology and calcium handling using *in vivo* and *in*
288 *situ* models. We show that the immature heart displays slowed atrioventricular conduction, prolonged
289 action potential duration time, and longer ventricular effective refractory periods, compared with adult
290 hearts. Age-dependent alterations in cardiac electrophysiology were associated with changes in genes
291 encoding voltage-gated potassium channels and intercalated disc proteins that facilitate intercellular
292 coupling and electrical propagation. Calcium handling was slowed in the immature heart, which
293 coincided with less developed excitation-contraction coupling machinery and an increased propensity
294 for calcium transient alternans.

295

296 Postnatal changes in cardiomyocyte morphology

297 Postnatal cardiac maturation includes the formation of intercellular connections between neighboring
298 cardiomyocytes, or intercalated discs. The cardiac intercalated disc includes the colocalization of
299 adherens junctions, desmosomes, gap junctions, sodium and potassium channels – which facilitates
300 the rapid transmission of electrical activity, initiating contractile forces between neighboring myocytes
301 (Noorman *et al.*, 2009; Wang *et al.*, 2012; Scuderi & Butcher, 2017). Indeed, the development of
302 intercellular low resistance pathways is vital to the heart's ability to function as a highly coordinated
303 syncytium. The spatial distribution of desmosomal, fascia adherens, and gap junction proteins shifts
304 throughout postnatal development, from sporadically distributed to densely concentrated at the terminal
305 ends of neighboring adult cardiomyocytes. In rodents, the intercalated discs are formed within the first

306 20 days after birth, but continue to develop well past maturity (Angst *et al.*, 1997). Conversely in
307 humans, the process is gradual with the colocalizing ion channels, adherens junctions, and gap
308 junctions not being apparent until 6-7 years after birth (Peters *et al.*, 1994; Vreeker *et al.*, 2014).

309
310 In the presented study, we reported an increase in the relative mRNA abundance of key genes involved
311 in intercellular connections and communication via the intercalated discs. From postnatal day 0 to 16,
312 older hearts had increased mRNA expression of connexin-43 (GJA1) typically localized to gap
313 junctions, as well desmosomal genes, including desmoplakin (DSP), plakoglobin (JPH2) and
314 junctophilin (JUP). Notably, well-established intercalated discs have a direct influence on electrical
315 conduction, and gap junction modifiers shorten ECG parameters and decrease the propensity for
316 cardiac alternans (Hsieh *et al.*, 2015). Similarly, we observed a progressive shortening of ECG
317 parameters (p-wave, PR interval) with postnatal age that coincided with increased expression of
318 intercalated disc genes.

319

320 Postnatal changes in excitation-contraction coupling

321 The immature heart transitions from hyperplasia to hypertrophic growth shortly after birth (Li *et al.*,
322 1996; Louch *et al.*, 2015) and as the cardiomyocytes increase in size, transverse tubules begin to form
323 and invaginate into the cell interior and the sarcoplasmic reticulum becomes more developed (Tanaka
324 *et al.*, 1998). These morphological changes facilitate the formation of dyads and couplons, wherein
325 ryanodine receptors and L-type calcium channels are in close proximity (Scriven *et al.*, 2013).
326 Concomitant with these organizational changes, cardiomyocytes become less dependent on the
327 sarcolemma calcium influx and more reliant on calcium-induced calcium release (Escobar *et al.*, 2004;
328 Ziman *et al.*, 2010; Hamaguchi *et al.*, 2013). Ziman, et al. correlated the timing of t-tubule and couplon
329 formation with improved excitation-contraction coupling in isolated cardiomyocytes aged 10 – 20 days
330 (Ziman *et al.*, 2010). The authors showed that myocytes up to PND 10 lacked a t-tubule system,
331 whereas the t-tubule system of cells isolated from PND 20 hearts were indistinguishable from adult
332 myocytes.

333

334 In the presented study, we observed a similar developmental time course, with increased mRNA
335 expression of calsequestrin, ryanodine and the sarcoplasmic reticulum calcium ATPase in hearts aged
336 10-16 days compared with 0-3 days. We also observed an age-dependent decrease in genes
337 associated with sarcolemma calcium influx – namely the sodium-calcium exchanger and T-type calcium
338 channel. Consequently, younger, immature hearts displayed prolonged calcium transient duration times
339 and an increased propensity for calcium transient alternans. Importantly, calcium alternans can be
340 associated with T-wave alternans and electrical instabilities (Clusin, 2003, 2008; Edwards & Blatter,
341 2014). Our results are in agreement with the work by Escobar, et al. which showed that ryanodine had

342 a negligible effect on 2-day old neonatal cardiomyocytes compared with cells isolated from 3-week old
343 juvenile animals (Escobar *et al.*, 2004). The latter indicates minimal involvement of calcium-induced
344 calcium release in the excitation-contraction coupling of immature hearts.

345

346 Postnatal changes in cardiac electrophysiology

347 Postnatal cardiac maturation in humans and rodents both include an increase in cell size, formation of
348 intercalated discs, invagination of t-tubules and increased dependence on calcium-induced calcium
349 release for excitation-contraction coupling. One of the inherent dissimilarities between species is an
350 age-dependent increase in the heart rate of small rodents (Heier *et al.*, 2010), which necessitates a
351 progressively shorter action potential as rodent cardiomyocytes mature (Escande *et al.*, 1985; Wahler
352 *et al.*, 1994; Wang *et al.*, 2003). In the presented study, we describe a linear increase in the heart rate
353 and shortening of ECG parameters in older vs younger animals. This time course corresponds with a
354 shift in myosin heavy chain expression to MYH6, which has kinetics that are three times faster than
355 MYH7 (Galler *et al.*, 2002). Although humans and rodents exhibit electrical restitution properties and an
356 action potential that is rate-dependent, the rodent action potential lacks a plateau phase due to
357 differences in outward potassium current (Knollmann *et al.*, 2007; Grandy *et al.*, 2007). We observed an
358 age-dependent increase in the expression of voltage-gated potassium channels – namely KCND2 and
359 KCND3 that encode Kv4.2 and Kv4.3 and facilitate I_{t_0} current. Indeed, I_{t_0} is responsible for >50% of
360 total outward potassium current and the very short APD that is characteristic of the adult mouse
361 myocardium (Wang *et al.*, 1996). In our study, action potentials showed rate dependency in all age
362 groups, but immature hearts displayed longer action potential duration times and ventricular effective
363 refractory periods.

364

365 Limitations

366 The scope of our study was limited to the age-dependent effects on cardiac electrophysiology and
367 calcium handling using a rat model, therefore differences with human physiology should be considered.
368 Despite many similarities, species-specific differences in cardiac physiology exist between rodents and
369 humans. Nevertheless, rodent models remain a valuable tool for understanding cardiac maturation, as
370 an ‘ideal’ human cardiac research model does not currently exist. Differentiated human embryonic stem
371 cells and induced pluripotent stem cells hold promise, but methodologies to reproducibly mature these
372 derived myocytes are still a work in progress (Feric & Radisic, 2016; Ruan *et al.*, 2016; Tiburcy *et al.*,
373 2017; Ronaldson-Bouchard *et al.*, 2018) and cell-based models cannot fully replicate a three-
374 dimensional whole heart. Further, since the presented study largely utilized an isolated heart model,
375 optical mapping data reflect developmental changes in myocardial physiology without neuronal input.

376

377 **CONCLUSION**

378 The mammalian heart continues to mature postnatally, with substantial developmental changes in
379 cardiac electrophysiology and calcium handling within the first few weeks after birth. This study utilized
380 in vivo recordings and an ex vivo heart model to characterize the developmental time course for
381 electrophysiology and calcium handling from postnatal day 0 – 14 and compared with adults. Results
382 of this study can serve as a baseline for future studies aimed at assessing environmental,
383 pharmacological or toxicological perturbations.

384 **REFERENCES**

- 385 Angst BD, Khan LU, Severs NJ, Whitely K, Rothery S, Thompson RP, Magee AI & Gourdie RG
386 (1997). Dissociated spatial patterning of gap junctions and cell adhesion junctions during
387 postnatal differentiation of ventricular myocardium. *Circ Res* **80**, 88–94.
- 388 Artman, Henry & Coetzee (2000). Cellular basis for age-related differences in cardiac
389 excitation-contraction coupling. *Prog Pediatr Cardiol* **11**, 185–194.
- 390 Bates KE et al. (2012). Pediatric cardiovascular safety: Challenges in drug and device
391 development and clinical application. *Am Heart J* **164**, 481–492.
- 392 Bers DM (2001). *Excitation-contraction coupling and cardiac contractile force*, Second.
393 Springer.
- 394 Bers DM (2002). Cardiac excitation-contraction coupling. *Nature* **415**, 198–205.
- 395 Cai B, Mu X, Gong D, Jiang S, Li J, Meng Q, Bai Y, Liu Y, Wang X, Tan X, Yang B & Lu Y
396 (2011). Difference of sodium currents between pediatric and adult human atrial myocytes:
397 evidence for developmental changes of sodium channels. *Int J Biol Sci* **7**, 708–714.
- 398 Clusin WT (2003). Calcium and cardiac arrhythmias: DADs, EADs, and alternans. *Crit Rev Clin*
399 *Lab Sci* **40**, 337–375.
- 400 Clusin WT (2008). Mechanisms of calcium transient and action potential alternans in cardiac
401 cells and tissues. *Am J Physiol - Hear Circ Physiol*.
- 402 Driscoll DJ, Gillette PC, Fukushige J, Lewis RM, Contant C, Hartley CJ, Entman ML, Schwartz
403 A & Dunn F (1980). Comparison of the cardiovascular action of isoproterenol, dopamine,
404 and dobutamine in the neonatal and mature dog. *Pediatr Cardiol* **1**, 307–314.
- 405 Edwards JN & Blatter LA (2014). Cardiac alternans and intracellular calcium cycling. *Clin Exp*
406 *Pharmacol Physiol* **41**, 524–532.
- 407 Escande D, Loisanche D, Planche C & Coraboeuf E (1985). Age-related changes of action
408 potential plateau shape in isolated human atrial fibers. *Am J Physiol* **249**, H843-50.
- 409 Escobar AL, Ribeiro-Costa R, Villalba-Galea C, Zoghbi ME, Pérez CG & Mejía-Alvarez R
410 (2004). Developmental changes of intracellular Ca²⁺ transients in beating rat hearts. *Am J*
411 *Physiol Heart Circ Physiol* **286**, H971-8.
- 412 Fedorov V V, Lozinsky IT, Sosunov EA, Anyukhovskiy EP, Rosen MR, Balke CW & Efimov IR
413 (2007). Application of blebbistatin as an excitation-contraction uncoupler for
414 electrophysiologic study of rat and rabbit hearts. *Hear Rhythm* **4**, 619–626.
- 415 Feric NT & Radisic M (2016). Maturing human pluripotent stem cell-derived cardiomyocytes in
416 human engineered cardiac tissues. *Adv Drug Deliv Rev* **96**, 110–134.
- 417 Galler S, Puchert E, Gohlsch B, Schmid D & Pette D (2002). Kinetic properties of cardiac
418 myosin heavy chain isoforms in rat. *Pflügers Arch Eur J Physiol* **445**, 218–223.
- 419 Grandy SA, Trépanier-Boulay V & Fiset C (2007). Postnatal development has a marked effect
420 on ventricular repolarization in mice. *Am J Physiol Circ Physiol* **293**, H2168–H2177.
- 421 Günthel M, Barnett P & Christoffels VM (2018). Development, Proliferation, and Growth of the
422 Mammalian Heart. *Mol Ther* **26**, 1599–1609.
- 423 Hamaguchi S, Kawakami Y, Honda Y, Nemoto K, Sano A, Namekata I & Tanaka H (2013).
424 Developmental changes in excitation-contraction mechanisms of the mouse ventricular
425 myocardium as revealed by functional and confocal imaging analyses. *J Pharmacol Sci*
426 **123**, 167–175.
- 427 Heier CR, Hampton TG, Wang D & DiDonato CJ (2010). Development of electrocardiogram
428 intervals during growth of FVB/N neonate mice. *BMC Physiol* **10**, 16.
- 429 Hondeghem LM, Carlsson L & Duker G (2001). Instability and triangulation of the action
430 potential predict serious proarrhythmia, but action potential duration prolongation is
431 antiarrhythmic. *Circulation* **103**, 2004–2013.

- 432 Hsieh Y-C, Lin J-C, Hung C-Y, Li C-H, Lin S-F, Yeh H-I, Huang J-L, Lo C-P, Haugan K, Larsen
433 BD, Wu T-J & Pharma Z (2015). Gap junction modifier rotigaptide decreases the
434 susceptibility to ventricular arrhythmia by enhancing conduction velocity and suppressing
435 discordant alternans during therapeutic hypothermia in isolated rabbit hearts. *Hear*
436 *Rhythm* **13**, 251–261.
- 437 Jaimes III R, Kuzmiak-Glancy S, Brooks DM & Kay MW (2014). Short Term Functional Effects
438 of Pyruvate Dehydrogenase Complex Activation in the Normoxic Heart. *Am J Physiol Hear*
439 *Circ Physiol*.
- 440 Jaimes R, Kuzmiak-Glancy S, Brooks D, Swift LM, Posnack NG & Kay MW (2016a).
441 Functional response of the isolated, perfused normoxic heart to pyruvate dehydrogenase
442 activation by dichloroacetate and pyruvate. *Pflügers Arch - Eur J Physiol* **468**, 131–142.
- 443 Jaimes R, Walton RD, Pasdois PLC, Bernus O, Efimov IR & Kay MW (2016b). A Technical
444 Review of Optical Mapping of Intracellular Calcium within Myocardial Tissue. *Am J Physiol*
445 *Heart Circ Physiol*ajpheart.00665.2015.
- 446 Kay M, Swift L, Martell B, Arutunyan A & Sarvazyan N (2008). Locations of ectopic beats
447 coincide with spatial gradients of NADH in a regional model of low-flow reperfusion. *Am J*
448 *Physiol Heart Circ Physiol* **294**, H2400--5.
- 449 Knollmann BC, Schober T, Petersen AO, Sirenko SG & Franz MR (2007). Action potential
450 characterization in intact mouse heart: steady-state cycle length dependence and
451 electrical restitution. *Am J Physiol Heart Circ Physiol* **292**, H614-21.
- 452 Krishnan A, Samtani R, Dhanantwari P, Lee E, Yamada S, Shiota K, Donofrio MT, Leatherbury
453 L & Lo CW (2014). A detailed comparison of mouse and human cardiac development.
454 *Pediatr Res* **76**, 500–507.
- 455 Lang D, Sulkin MS, Lou Q & Efimov IR (2011). Optical Mapping of Action Potentials and
456 Calcium Transients in the Mouse Heart. *J Vis Exp*.
- 457 Li F, Wang X, Capasso JM & Gerdes AM (1996). Rapid Transition of Cardiac Myocytes from
458 Hyperplasia to Hypertrophy During Postnatal Development. *J Mol Cell Cardiol* **28**, 1737–
459 1746.
- 460 Louch WE, Koivumäki JT & Tavi P (2015). Calcium signalling in developing cardiomyocytes:
461 implications for model systems and disease. *J Physiol* **593**, 1047–1063.
- 462 Mahdavi V, Lompre AM, Chambers AP & Nadal-Ginard B (1984). Cardiac myosin heavy chain
463 isozymic transitions during development and under pathological conditions are regulated
464 at the level of mRNA availability. *Eur Heart J* **5 Suppl F**, 181–191.
- 465 Marcela SG, Cristina RMM, Angel PGM, Manuel AM, Sofia D-C, Patricia DLR-S, Bladimir R-R
466 & Concepción SG (2012). Chronological and Morphological Study of Heart Development
467 in the Rat. *Anat Rec Adv Integr Anat Evol Biol* **295**, 1267–1290.
- 468 Mollova M, Bersell K, Walsh S, Savla J, Das LT, Park S-Y, Silberstein LE, dos Remedios CG,
469 Graham D, Colan S & Kühn B (2013). Cardiomyocyte proliferation contributes to heart
470 growth in young humans. *Proc Natl Acad Sci* **110**, 1446–1451.
- 471 Noorman M, van der Heyden MAG, van Veen TAB, Cox MGPJ, Hauer RNW, de Bakker JMT &
472 van Rijen HVM (2009). Cardiac cell–cell junctions in health and disease: Electrical versus
473 mechanical coupling. *J Mol Cell Cardiol* **47**, 23–31.
- 474 Obreztkhikova MN, Sosunov EA, Plotnikov A, Anyukhovskiy EP, Gainullin RZ, Danilo P, Yeom
475 Z-H, Robinson RB & Rosen MR (2003). Developmental changes in IKr and IKs contribute
476 to age-related expression of dofetilide effects on repolarization and proarrhythmia.
477 *Cardiovasc Res* **59**, 339–350.
- 478 Pesco-Koplowitz L, Gintant G, Ward R, Heon D, Saulnier M & Heilbraun J (2018). Drug-
479 induced cardiac abnormalities in premature infants and neonates. *Am Heart J* **195**, 14–38.
- 480 Peters NS, Severs NJ, Rothery SM, Lincoln C, Yacoub MH & Green CR (1994).

- 481 Spatiotemporal relation between gap junctions and fascia adherens junctions during
482 postnatal development of human ventricular myocardium. *Circulation* **90**, 713–725.
- 483 Posnack NG, Jaimes R, Asfour H, Swift LM, Wengrowski AM, Sarvazyan N & Kay MW
484 (2014a). Bisphenol A exposure and cardiac electrical conduction in excised rat hearts.
485 *Environ Health Perspect* **122**, 384–390.
- 486 Posnack NG, Jaimes R, Asfour H, Swift LM, Wengrowski AM, Sarvazyan N, Kay MW, Jaimes
487 III R, Asfour H, Swift LM, Wengrowski AM, Sarvazyan N, Kay MW, Jaimes R, Asfour H,
488 Swift LM, Wengrowski AM, Sarvazyan N & Kay MW (2014b). Bisphenol A Exposure and
489 Cardiac Electrical Conduction in Excised Rat Hearts. *Environ Health Perspect* **122**, 384–
490 390.
- 491 Racca AW, Klaiman JM, Pioner JM, Cheng Y, Beck AE, Moussavi-Harami F, Bamshad MJ &
492 Regnier M (2016). Contractile properties of developing human fetal cardiac muscle. *J*
493 *Physiol* **594**, 437–452.
- 494 Ramadan M, Sherman M, Jaimes R, Chaluvadi A, Swift L, Posnack NGNG & Posnack NGNG
495 (2018). Disruption of neonatal cardiomyocyte physiology following exposure to bisphenol-
496 a. *Sci Rep* **8**, 7356.
- 497 Robinson RB (1996). Autonomic receptor--effector coupling during post-natal development.
498 *Cardiovasc Res* **31 Spec No**, E68-76.
- 499 Ronaldson-Bouchard K, Ma SP, Yeager K, Chen T, Song L, Sirabella D, Morikawa K, Teles D,
500 Yazawa M & Vunjak-Novakovic G (2018). Advanced maturation of human cardiac tissue
501 grown from pluripotent stem cells. *Nature* **556**, 239–243.
- 502 Ruan J-L, Tulloch NL, Razumova M V., Saiget M, Muskheli V, Pabon L, Reinecke H, Regnier
503 M & Murry CE (2016). Mechanical Stress Conditioning and Electrical Stimulation Promote
504 Contractility and Force Maturation of Induced Pluripotent Stem Cell-Derived Human
505 Cardiac Tissue. *Circulation* **134**, 1557–1567.
- 506 Saul J, Ross B, Schaffer MS, Beerman L, Melikian AP, Shi J, Williams J, Barbey JT, Jin J,
507 Hinderling PH & Pediatric Sotalol Investigators (2001). Pharmacokinetics and
508 pharmacodynamics of sotalol in a pediatric population with supraventricular and
509 ventricular tachyarrhythmia. *Clin Pharmacol Ther* **69**, 145–157.
- 510 Scriven DRL, Asghari P & Moore EDW (2013). Microarchitecture of the dyad. *Cardiovasc Res*
511 **98**, 169–176.
- 512 Scuderi GJ & Butcher J (2017). Naturally Engineered Maturation of Cardiomyocytes. *Front cell*
513 *Dev Biol* **5**, 50.
- 514 Spach MS, Heidlage JF, Dolber PC & Barr RC (2000). Electrophysiological effects of
515 remodeling cardiac gap junctions and cell size: experimental and model studies of normal
516 cardiac growth. *Circ Res* **86**, 302–311.
- 517 Swift L, Martell B, Khatri V, Arutunyan A, Sarvazyan N & Kay M (2008). Controlled regional
518 hypoperfusion in Langendorff heart preparations. *Physiol Meas* **29**, 269–279.
- 519 Swift LMLM, Asfour H, Posnack NGNG, Arutunyan A, Kay MWMW & Sarvazyan N (2012).
520 Properties of blebbistatin for cardiac optical mapping and other imaging applications.
521 *Pflugers Arch Eur J Physiol* **464**, 503–512.
- 522 Tanaka H, Sekine T, Nishimaru K & Shigenobu K (1998). Role of sarcoplasmic reticulum in
523 myocardial contraction of neonatal and adult mice. *Comp Biochem Physiol A Mol Integr*
524 *Physiol* **120**, 431–438.
- 525 Tiburcy M et al. (2017). Defined Engineered Human Myocardium With Advanced Maturation
526 for Applications in Heart Failure Modeling and Repair. *Circulation* **135**, 1832–1847.
- 527 Vreeker A, van Stuijvenberg L, Hund TJ, Mohler PJ, Niekels PGJ & van Veen TAB (2014).
528 Assembly of the Cardiac Intercalated Disk during Pre- and Postnatal Development of the
529 Human Heart ed. Goumans MJ. *PLoS One* **9**, e94722.

- 530 Wagner MB, Wang Y, Kumar R, Tipparaju SM & Joyner RW (2005). Calcium Transients in
531 Infant Human Atrial Myocytes. *Pediatr Res* **57**, 28–34.
- 532 Wahler GM, Dollinger SJ, Smith JM & Fleml KL (1994). Time course of postnatal changes in
533 rat heart action potential and in transient outward current is different. *Am J Physiol Circ*
534 *Physiol* **267**, H1157–H1166.
- 535 Wang L & Duff HJ (1997). Developmental Changes in Transient Outward Current in Mouse
536 Ventricle. *Circ Res* **81**, 120–127.
- 537 Wang L, Feng Z-P, Kondo CS, Sheldon RS & Duff HJ (1996). Developmental Changes in the
538 Delayed Rectifier K⁺ Channels in Mouse Heart. *Circ Res*.
- 539 Wang Q, Lin JL-C, Wu K-H, Wang D-Z, Reiter RS, Sinn HW, Lin C-I & Lin C-JJ (2012). Xin
540 proteins and intercalated disc maturation, signaling and diseases. *Front Biosci (Landmark*
541 *Ed* **17**, 2566–2593.
- 542 Wang Y, Xu H, Kumar R, Tipparaju SM, Wagner MB & Joyner RW (2003). Differences in
543 transient outward current properties between neonatal and adult human atrial myocytes. *J*
544 *Mol Cell Cardiol* **35**, 1083–1092.
- 545 van Weerd JH & Christoffels VM (2016). The formation and function of the cardiac conduction
546 system. *Development* **143**, 197–210.
- 547 Ziman AP, Gómez-Viquez NL, Bloch RJ & Lederer WJ (2010). Excitation-contraction coupling
548 changes during postnatal cardiac development. *J Mol Cell Cardiol* **48**, 379–386.

549

550

551 **DISCLOSURES:** Nothing to disclose.

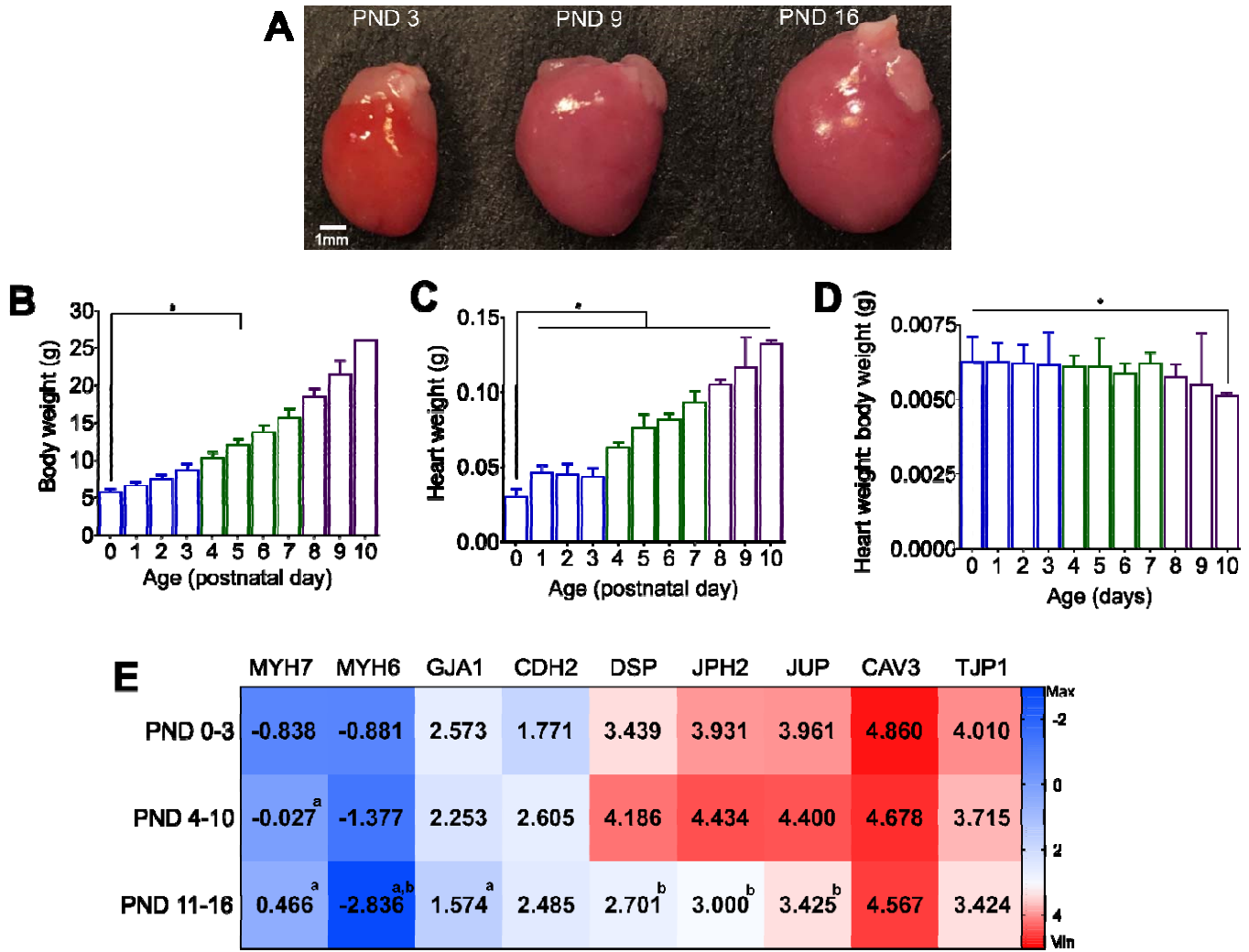
552 **FUNDING:** This work was supported by the National Institutes of Health (R00ES023477 &
553 R01HL139472 to NGP), Children’s Research Institute and Children’s National Heart Institute.

554 **AUTHOR CONTRIBUTIONS:** LS, MB, DG, MR¹, MR², DM, AC, CM, RJ and NGP performed
555 experiments; LS, MB, DG, MR¹, MR², DM, AC, CM, RJ and NGP analyzed data; LS, MB, DG, MR¹, RJ
556 and NGP prepared figures; NGP drafted manuscript; LS, MB, RJ and NGP conceived and designed
557 experiments; LS, MG, DG, MR¹, MR², DM, AC, CM, RJ and NGP approved manuscript. ¹Manelle
558 Ramadan, ²Marissa Reilly

559 **FIGURES**

560

561



562

563

564

565 **Figure 1. Postnatal development and cardiac maturation**

566 **(A)** Isolated whole hearts from postnatal day 3, 9 and 16. **(B)** Age-dependent increase in body weight

567 and **(C)** heart weight, and **(D)** slight decrease in the heart weight to body weight ratio. **(E)**

568 Developmental time course corresponds to shift in myosin heavy chain gene expression (*MYH7* to

569 *MYH6*), and increased expression of key genes involved in intercellular coupling via gap junctions

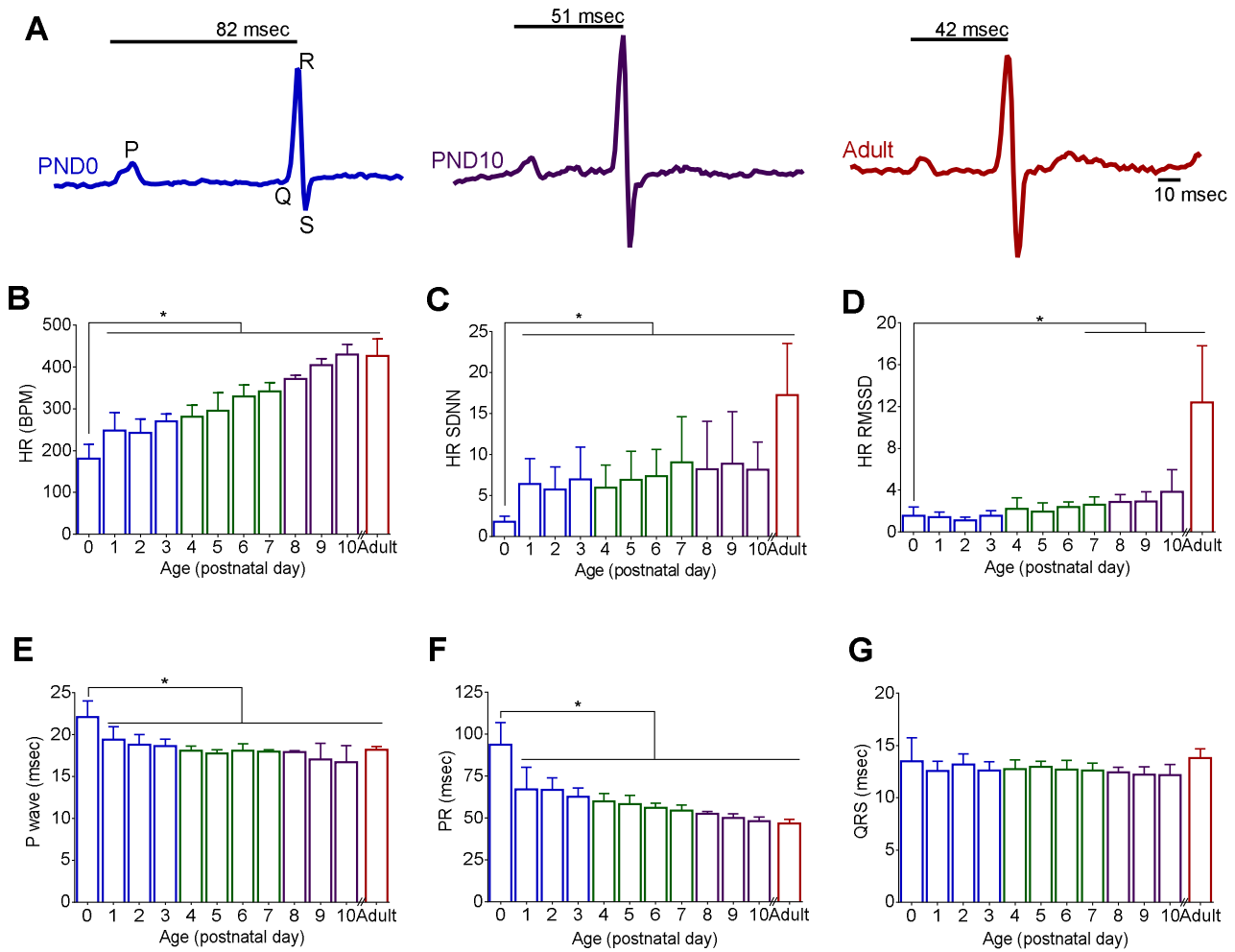
570 (*GJA1*) and desmosomes (*DSP*, *JPH2*, *JUP*). Gene expression scale depicts maximal expression

571 across all genes in this cohort (blue) and minimal expression (red), relative to *GAPDH* housekeeping

572 gene. PND = postnatal day; 'a' denotes significant difference relative to PND 0-3 age, 'b' denotes

573 significant difference relative to PND 4-10 age. mean \pm SD, $n \geq 3$ independent experiments.

574



575

576

577 **Figure 2. Age-dependent alterations in *in vivo* electrocardiogram parameters**

578 **(A)** Example of non-invasive electrocardiogram waveforms recorded from postnatal day 0 (PND 0), 10

579 (PND 10) and adult animal; PR interval time is denoted. Postnatal development was associated with an

580 age-dependent increase in heart rate **(B)**, heart rate variability **(C,D)**, shortening of p-wave duration **(E)**

581 and shortening of the PR interval **(F)**. No significant difference in the QRS interval time was observed

582 using non-invasive recordings **(G)**. *indicates statistically significant difference from earliest measured

583 time point (PND 0). PND = postnatal day, $n \geq 7$ animals per age, mean \pm SD, * $p < 0.05$

584

585

586

587

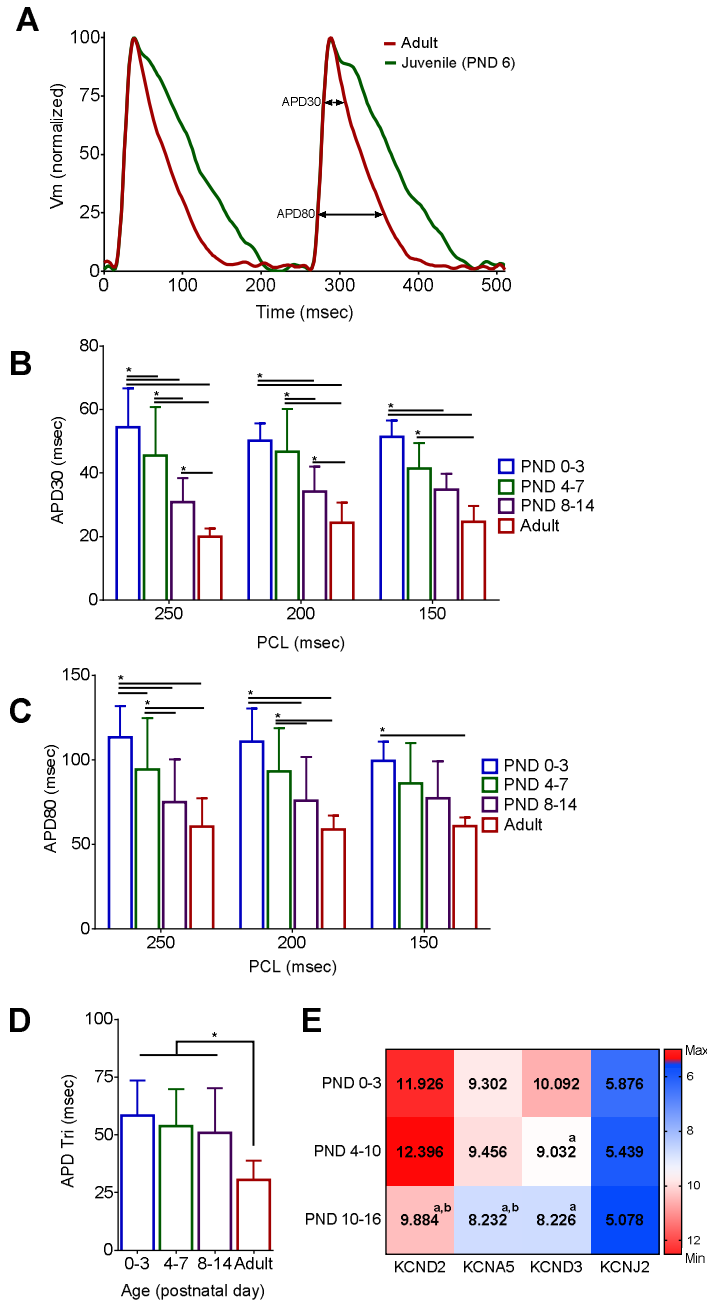
588

589

590

591

592



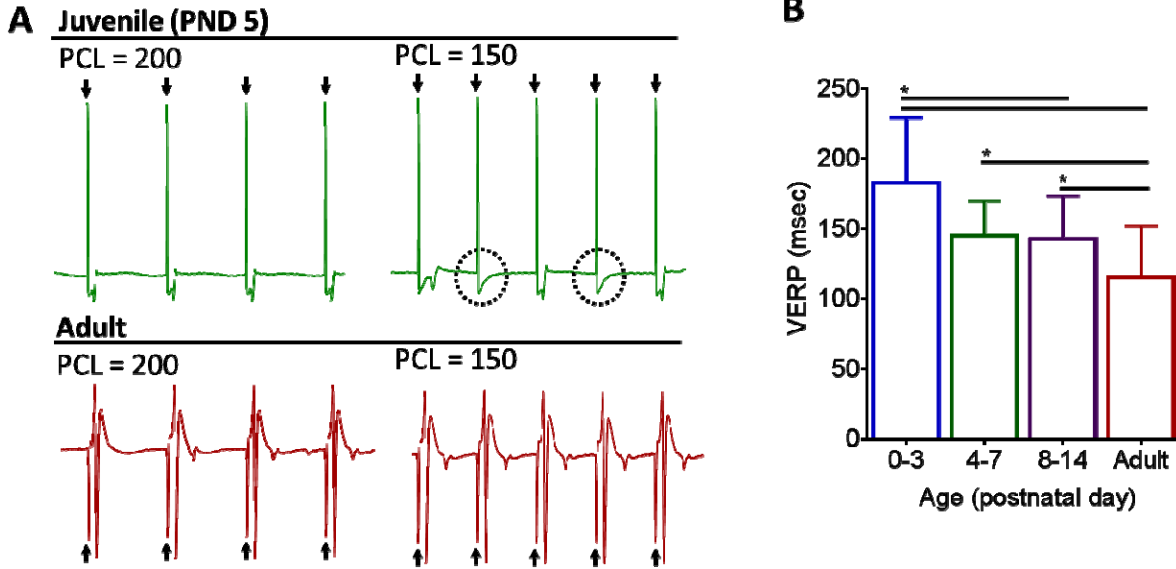
593 **Figure 3. Age-dependent shortening of action potential duration time**

594 **(A)** Transmembrane voltage (Vm) signals optically mapped from the epicardial surface of excised,
 595 intact hearts (250 msec PCL). **(B,C)** Prolonged APDs were observed in younger hearts (APD30,
 596 APD80), which also displayed more triangulated action potentials **(D)**. Shortened APD in older animals
 597 coincided with an age-dependent increase in voltage-gated potassium channel gene expression **(E)**.
 598 Data binned into the following age groups: PND 0-3, PND 4-7, PND 8-14 and adult (2-3months). $n \geq 5$
 599 individual hearts per age. APD30 = action potential duration at 30% repolarization, APD80 = 80%

600 repolarization, APD Tri = Triangulation APD80-APD30, PND = postnatal day. $n \geq 7$ animals per age,
601 mean \pm SD, * $p < 0.05$

602

603



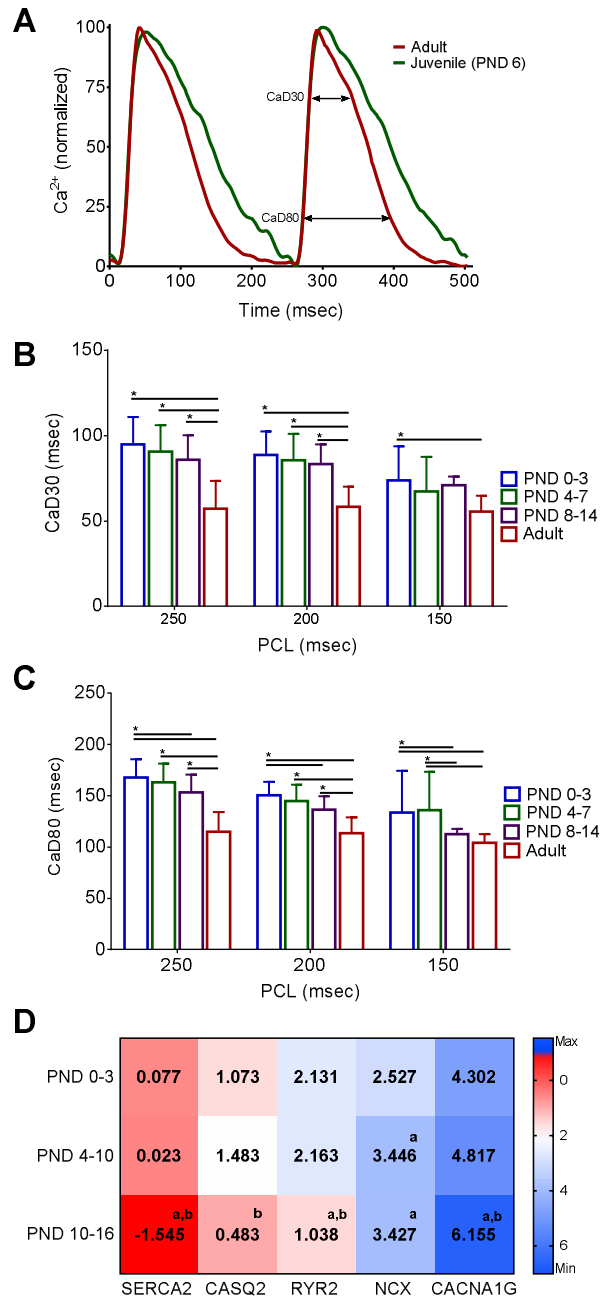
604

605 **Figure 4. Age-dependent shortening of the ventricular effective refractory period (VERP)**

606 **(A)** Excised hearts were paced near the apex at two pacing cycle lengths (PCL = 250 msec, 150 msec)
607 and electrocardiograms were recorded. Pacing spikes denoted with arrows. Top: Juvenile heart at both
608 PCL. Note the loss of capture, circled, at a shorter cycle length. Bottom: Adult heart shows ventricular
609 response to each pacing spike, at both pacing frequencies. **(B)** Age-dependent decrease in the VERP.

610 $n \geq 5$ animals per age, mean \pm SD, * $p < 0.05$

611



612 **Figure 5. Age-dependent shortening of calcium handling**

613 **(A)** Calcium transients recorded from the epicardial surface of excised, intact hearts (250 msec PCL).

614 **(B,C)** Prolonged CaDs were observed in younger hearts (CaD30, CaD80). Faster calcium handling in

615 older animals coincided with an age-dependent increase in key calcium handling genes associated with

616 calcium binding in the sarcoplasmic reticulum (CASQ2), calcium release (RYR), calcium reuptake into

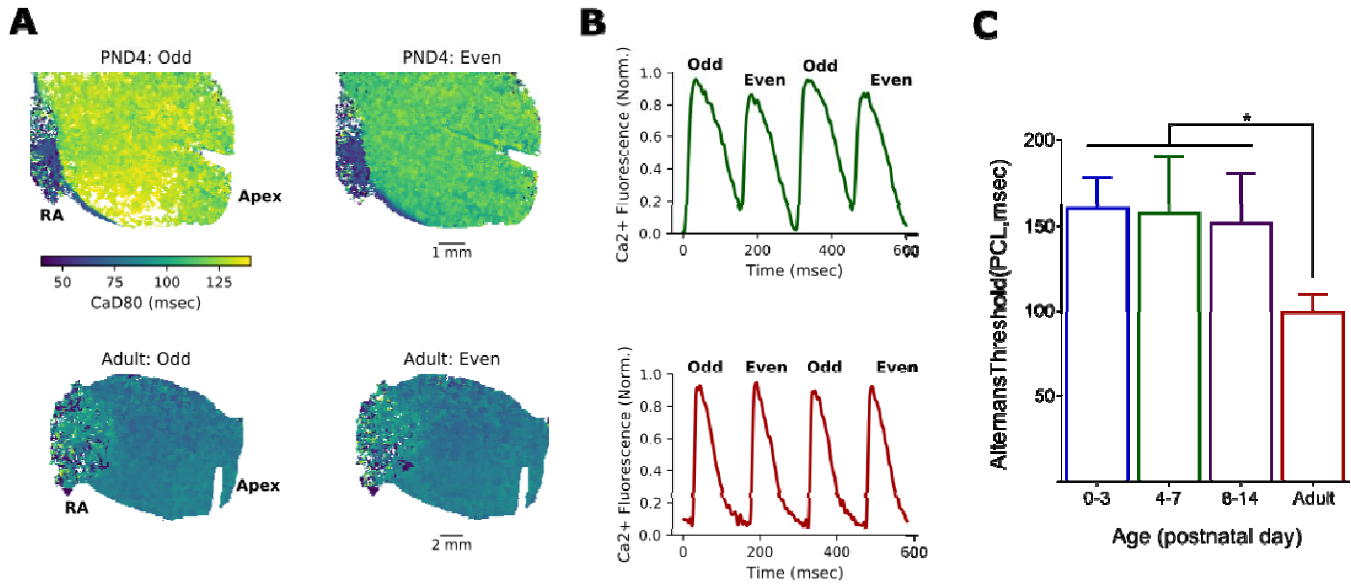
617 the SR (SERCA2) and an age-dependent decrease in the sodium-calcium exchanger (NCX) and

618 immature T-type calcium channels (CACNA1G). Data binned into the following age groups: PND 0-3,

619 PND 4-7, PND 8-14 and adult (2-3 months). $n \geq 5$ individual hearts per age. CaD30 = calcium transient

620 duration at 30%, CaD80 = 80%, PND = postnatal day. $n \geq 7$ animals per age, mean \pm SD, * $p < 0.05$

621
622



623
624
625
626
627

Figure 6. Increased incidence of calcium transient alternans in immature hearts

628 **(A)** Immature hearts (top two panels) displayed an increased susceptibility to calcium transient
629 alternans compared with adult hearts (bottom two panels). Images show peak fluorescence at 150
630 msec PCL. **(B)** Green and red traces represent four paced beats from the neonatal (PND4) and adult
631 heart, respectively. **(C)** The slowest PCL that resulted in alternating calcium transients (alternans
632 threshold) was significantly slower in younger hearts compared with adults. Data binned into the
633 following age groups: PND 0-3, PND 4-7, PND 8-14 and adult (2-3months). PND = postnatal day. $n \geq 6$
634 animals per age, mean \pm SD, * $p < 0.05$

635